Geotechnical Testing Journal, Vol. 31, No. 5
Paper ID GTJ101367
Available online at: www.astm.org

C. Comina,[1] *S. Foti,*[2] *G. Musso,*[3] *and E. Romero*[4]

EIT Oedometer: An Advanced Cell to Monitor Spatial and Time Variability in Soil with Electrical and Seismic Measurements

ABSTRACT: The paper presents an innovative oedometer cell (EIT oedometer), accomplishing for monitoring the spatial and temporal evolution of different physical quantities inside soil samples through seismic and electric non-destructive measurements. The technical solutions implemented to perform correct electrical measurements are reported together with the results of benchmark tests demonstrating the potentialities and the limits of the 3D electrical resistivity tomography in detecting both pre-existing and induced sample heterogeneities. It is shown that resistivity imaging can offer a powerful tool for the investigation of soil heterogeneities not detected by external measurements. The relationship between electrical resistivity and soil properties makes this application potentially useful for monitoring the evolution of transient processes as for instance those related to the diffusion of chemical species in clay soils and associated coupled chemo-mechanical processes, whereas the information gathered by classical oedometer measurements and by seismic waves propagation could be used to explore the associated macroscopic phenomena.

KEYWORDS: electric tomography, geophysical laboratory testing, hydro-chemo-mechanical processes

Introduction

In traditional soil mechanics tests, stresses and strains are extrapolated on the basis of measurements that are averaged over the whole soil specimen (e.g., global measurements in triaxial tests using external transducers). The intrinsic limit of this approach consists in the fact that specimens are represented as homogeneous both with respect to their initial conditions and regarding their responses to transitory processes.

The need for models and experiments incorporating heterogeneities in the representative volume of soils stems from a number of phenomena of increasing interest in geotechnical engineering. Testing induced heterogeneity can be of mechanical nature, for example, the localization of deformations in shear bands, or due to changes in hydraulic forces (pressure in saturated soils, suction in unsaturated ones) or chemistry (variation of concentration of chemical species, dissolution-precipitation); most of them inducing both mechanical consequences (e.g., deformations of osmotic nature) and hydraulic variations (e.g., preferential flow paths of the liquid or gaseous phases). Indeed, many recent phenomenological models for the study of processes in complex materials postulate the existence of different scales of interaction (e.g., Gens and Alonso 1992). In most cases available experimental equipment is, however, not suitable for calibrating these models by means of simultaneous measurements of the processes at the postulated scales.

Manuscript received August 1, 2007; accepted for publication March 2, 2008; published online April 2008.

[1]Research Associate, Dipartimento di Ingegneria Strutturale e Geotecnica, Politecnico di Torino, 10129 Italy; e-mail: cesare.comina@polito.it

[2]Assistant Professor, Dipartimento di Ingegneria Strutturale e Geotecnica, Politecnico di Torino, 10129 Italy; e-mail: sebastiano.foti@polito.it

[3]Assistant Professor, Dipartimento di Ingegneria Strutturale e Geotecnica, Politecnico di Torino, 10129 Italy; e-mail: guido.musso@polito.it. Formerly Eni E&P Division-TERA, Milano, Italy.

[4]Head of Geotechnical Laboratory, Universitat Politècnica de Catalunya, 08034 Barcelona, Spain, e-mail: enrique.romero-morales@upc.edu

To overcome this intrinsic limitation, different approaches have been attempted by imaging soil specimens' behavior with a variety of techniques. In particular, to determine flow pathways in natural soils, magnetic resonance imaging (Amin et al. 1993; Hedburg et al. 1993), x-ray tomography and dual-energy gamma-ray methods (Anderson et al. 1992; Peyton et al. 1992; Rolland et al. 2005; Van Geet et al. 2005; Rodríguez-Rey et al. 2006) have been used. These techniques provide small-scale resolution and are able to identify tiny features such as small fissures and cracks but are very expensive and not widely available.

In contrast, electric resistivity methods are relatively cost effective and fast in terms of data acquisition times; moreover, they may also be applied to a wide range of scales. In this respect they are widely used for *in situ* testing. Various relationships (see, e.g., Pfannkuch 1969; Mitchell 1993; Berryman 1995) can be found in the literature relating the electrical resistivity of saturated soils to the physico-chemical properties of the mixture (concentration of ionic species, porosity, tortuosity, specific surface, cation exchange capacity). Laboratory applications have been recently proposed to estimate the evolution of the degree of saturation in column tests of pollutant infiltration (Kamon et al. 2003), to monitor sedimentation and consolidation processes (McCarter and Desmazes 1997; Blewett et al. 2001), and to study soil liquefaction (Jinguuji et al. 2007). Such investigations were, however, limited to the study of mono-dimensional problems and were not able to estimate the variability of the electric field across the specimens, associated with local variations of soil characteristics.

More information can be obtained if the electrical measurements are used for tomographic reconstruction of the resistivity field, as widely done in geophysical prospecting (Reynolds 1997). Electrical resistive tomography (ERT) is a technique that allows estimation of the spatial distribution of the electrical resistivity (or its inverse, conductivity) within an object from impedance measurements at its boundaries. Usually several electrodes are applied to the surface of the object and known currents are imposed on some of them. The voltages resulting from the application of such cur-

rents are then measured on the remaining electrodes. Since the collected measurements are linked to the object conductivity by known physical laws, it is possible to estimate the distribution of conductivity within the object by solving an inverse problem.

The application of such a technique to laboratory experiments is quite new, although some preliminary studies can be found in the literature (Binley et al. 1996; Olsen et al. 1999; and Sambuelli et al. 2002). Laboratory investigations of 2D imaging of soils specimens with electric tomography have been very successful in locating various types of heterogeneities (clay content, compaction characteristics, and grain size distribution; Borsic et al. 2005) and in monitoring the diffusion of saline solutions in sand samples (Comina et al. 2005; Damasceno and Fratta 2006).

On a complementary side, seismic wave velocity measurement using piezoceramic elements has become of common application in most geotechnical laboratories (Brignoli et al. 1996; Jovicic et al. 1996; Lee and Santamarina 2006) and can provide important information about the mechanical properties of the soil skeleton. The mutual relationships among electrical, seismic, and mechanical properties of clay soils undergoing chemical diffusion has been shown in one-dimensional conditions for instance by Santamarina and Fam (1995).

The present paper presents a new advanced oedometer cell, which allows for 3D electric tomography and seismic wave velocity measurements. In the first part of the paper, the cell itself and the associated tools for resistivity measurements and tomographic analyses are described, with special emphasis on the design issues necessary for running electrical measurements. Successively, some benchmark tests are reported to illustrate the capability of tomographic imaging. Finally, the results of an oedometer test on a sand specimen are reported to show the performance of the apparatus.

EIT Oedometer

Implementing electrical measurements in laboratory equipment is a rather challenging task because all the possible electrical shortcuts within the cell structure must be prevented to measure the electrical resistivity of the sample. In this respect, the presence of the pore fluid requires special attention in the design process of the apparatus. Other requirements are related to the correct location of seismic sensors for wave propagation measurements and to the necessity of having a stiff structure with respect to oedometer conditions. These issues have been accomplished by adopting specific design and construction techniques as described in the following sections.

Cell Description

The loading scheme of the cell is the classical one of oedometers, in which a vertical load is applied to the sample under lateral confinement. Moreover, by adopting concepts already developed for an existing controlled suction oedometer (Romero et al. 1995), different paths in terms of stresses, hydraulic pressure, and relative humidity can be imposed on the specimen.

Geometrical dimensions have been chosen to limit the influence of side boundaries, which can cause wave reflections and refractions (Lee and Santamarina 2006; Comina 2005). An internal diameter of 130 mm has therefore been adopted. Consequently, to ensure proper one-dimensional conditions, hosted samples shall have heights ranging from 20 to 60 mm (Fig. 1).

The inner walls of the oedometer are completely covered by an

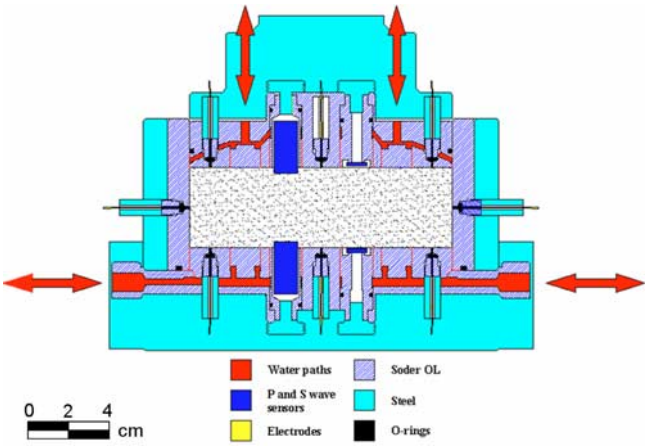

FIG. 1—*Cross section of the EIT oedometer cell.*

insulating and stiff polyamide plastic material (commercial denomination SÖDER-ÖL with resistivity of approximately 10^{13} Ωm) to ensure the correct measurement of the electrical potential. The insulating polyamide also ensures a reduced ring friction effect. The external structure of the cell is instead constituted by steel to guarantee the adequate overall stiffness. In Fig. 2 some pictures of the cell are reported.

To avoid the presence of conductive elements that would cause electrical bridges on the cell top and bottom caps, and in order to allow for the placement of electrodes, drainage is obtained by concentric rings having a tolerance of few micrometers between each of them (Fig. 3). The permeability of these caps has been evaluated by performing flow tests under constant gradient conditions, inducing flows towards both the interior and the exterior of the cell. The measured equivalent permeability was about 6×10^{-6} m/s for both caps.

For ERT measurements, 42 electrodes are hosted on the internal boundary of the cell (16 electrodes equally spaced on the sidewall at a height of 20 mm from the bottom cap and 13 on each cap). The presence of electrodes on the bases increases the amount of information related to the central portion of the sample, where typically the resolution of the inverse problem is poor. To further increase the sensitivity of the electrical inversion, electrodes on the caps are not

FIG. 2—*EIT oedometer cell: (a) external view of the cell and loading system and (b) particulars of metallic confining ring and insulating internal material.*

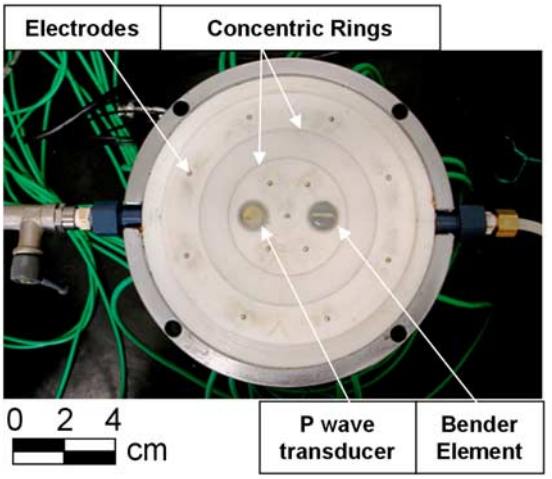

FIG. 3—*EIT oedometer cell. Bottom base with P, S wave transducers and electrode disposition. Drainage paths are created through the tolerance between concentric rings.*

equally spaced but concentrated near the center (Fig. 3). The electrodes are thin brass threads with a head of 2 mm diameter. Since fluids in the cell can be back-pressurized, leakage has been prevented by waterproofing the electrode ports using connections for each electrode with pressed o-rings that are screwed against the inner non-conductive cell wall (Fig. 4).

A fundamental requirement for execution of electric tomographies is to avoid the contact between the interstitial water of samples and the external steel structure of the cell. Hence, all the water paths have been covered by plastic insulators and two o-rings have been placed around the bottom and top cap of the cell (Fig. 1). The top o-ring is expected to develop some friction during loading so that the externally applied load has to be adjusted to account for this effect. A calibration in this respect has been performed by applying mechanical load on the empty cell against a load cell. The effect of friction has been estimated to be of few kPa, so that it can be easily taken into consideration in the interpretation of tests.

Sensors for the measurement of P and S wave velocity have been allocated on top and bottom caps of the cell. For S wave measurements cantilever mounted PZT-5A Bimorphs by Morgan Electro Ceramics (10 by 20 by 0.5 mm^3) with a parallel connection have been used. These elements are tied up at their extremity for approximately 1/3 of the length and protrude in the sample for about 5 mm. In order to separate them from the base (avoiding generating a wave in the structure of the cell), a silicon injection is made around the elements.

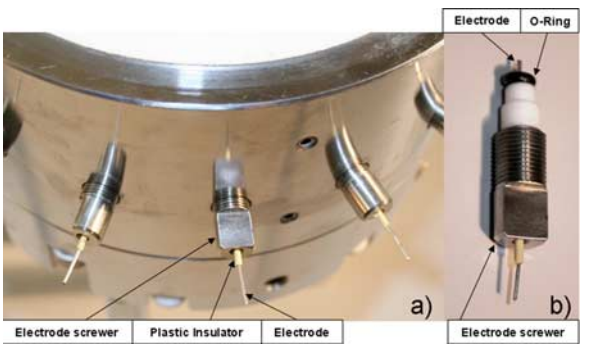

FIG. 4—*Electrode connection: (a) Overall view of the circumferential ring and (b) detail of a single electrode.*

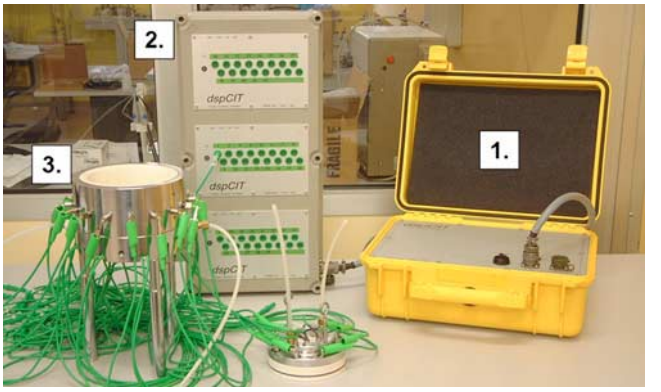

FIG. 5—*Measurement setup: 1. Complex impedance tomograph. 2. Multiplexers and connection to the cell. 3. EIT oedometer cell.*

The transducers used to generate and receive P waves are a lead zirconate titanate ceramic PZT-5A with a cylindrical shape. The ceramic element is produced by Physik Instrument with a thickness of 2 mm and a diameter of 8 mm. The wires are welded on the top and bottom faces of the element in order to provide vertical movement.

Both seismic sensors are allocated in an opposite space in the bases and covered by a thin surface of epoxy in order to insulate the piezoceramic from interstitial water. Figure 3 reports the picture of the bottom base of the cell where both the bender element and the P wave sensor are installed with their epoxy cover; the top base is similarly constructed. The slots for seismic sensors have been designed in order to be easily removed, providing room for other transducers (e.g., thermocouples). Alternatively, the same slots can also be used to induce external perturbations in the soil sample (e.g., infiltration or extraction of fluids).

Acquisition Devices

The execution of resistivity measurements for tomography requires the injection of current at two electrodes, while other pairs of electrodes are used to measure the electric potentials. The complex impedance tomograph (CIT, Fig. 5) used for injecting currents and acquiring potential has been constructed by Iridium Italy s.a.s.; its main characteristics are reported in Table 1. It is a very fast acquisition device with 16-bit resolution. Indeed, the instrument can perform approximately 200 acquisitions per second (at an operating frequency of 1 kHz) so that it is possible to measure water content or concentration variations also for relatively fast transient phenomena. The device has been constructed in order to be suitable also for field tests so that a direct comparison of laboratory and *in situ* tests is possible. For example, the CIT has been successfully

TABLE 1—*Complex impedance tomograph characteristics.*

COMPLEX IMPEDANCE TOMOGRAPH	
Maximum output current	±250 mA (500 mApp)
Maximum output voltage	±50 V (100 Vpp)
Operative frequencies	0.1 to 2500 Hz
Acquisition channels	48
Resolution on phase angles	≈1 mrad
Resolution on voltage	100 μV
Resolution on current	10 μA
Input impedance	200 MΩ

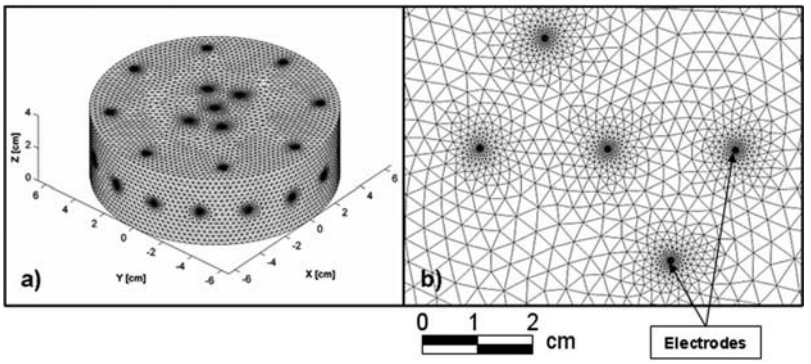

FIG. 6—*Finite element mesh: (a) global view and (b) zoom close to top cap electrodes.*

applied for the characterization of trees, where high conductivity is associated with degraded zones (Sambuelli et al. 2003). The tomograph is connected with the electrodes of the cell by means of three multiplexers (one for the circumferential electrodes, the other two, respectively, for top and bottom bases).

The tomograph is controlled by a PC, which is used to set the excitations and to gather the experimental data. Seismic wave acquisition is managed by the use of two different National Instruments boards installed on the same PC: a NI PCI-6731 analog output board for exciting the piezoceramic elements and a NI PCI-4452 DSA board for acquiring the waveforms.

Software

Reconstruction of the conductivity distribution inside the samples is made through a software that is a generalization, to 3D geometry, of the one used in previous 2D experiences (Borsic et al. 2005; Comina et al. 2005). It is a commercial tool developed by Sc-Aip (www.scaip.com) that implements a least-squares inversion algorithm with Tikonov regularization, solving the forward problem stated by Maxwell's equations with a finite element approach. The mesh used for the present application is composed of 32 945 tetrahedrons and is more refined in the proximity of the electrodes (Fig. 6), in order to catch with proper care the sharp electrical field generated around them. Indeed, in these zones of the sample there are abrupt potential changes, due to the injected currents from the surface of electrodes to the soil. For the same reason, electrodes are modeled with their actual size and not as dimensionless points, according to the Complete Electrode Model (Somersalo et al. 1992), taking into account also the contrast of impedance with respect to the surrounding soil. The average size of the elements is about 0.25 cm. This dimension fixes the resolution of the reconstruction process.

The mesh reflects the initial geometry of the sample; hence, when testing highly deformable materials, it is necessary to update the mesh during the evolution of the test to adapt it to the new geometrical configuration.

Optimization of the Acquisition Protocol for 3D ERT

The initial problem to be addressed for 3D electric tomography was the choice of the optimal measuring protocol. Indeed, no 3D patterns of acquisition are available in the literature for the complex electrode disposition chosen for this oedometer. The number of electrodes used in ERT is usually limited by available surface area, data acquisition complexities, and data acquisition/reconstruction times (dependent on measurement strategy or utilization of available electrodes). Most of 3D electric tomographies involve "conventional" arrangements of electrodes in circumferential rings at different heights around the wall of the cell (Borsic 2002; Murphy et al. 2006).

To track transient phenomena, the optimal measuring sequence should represent a compromise between resolution and speed of acquisition. To satisfy the first need, a great number of voltage readings should be run in order to fully characterize the sample. On the other hand, measurements are time consuming, so that their number should be limited in order to catch an "instantaneous" picture.

Acquisition times can be reduced keeping in mind that not all the possible combinations of injecting and measurement electrode pairs lead to independent measurements. A brute force acquisition scheme, using all the possible pairs, would lead to redundant information not useful for the reconstruction process. The total number of independent measures N is given by (Noel and Xu 1991):

$$N = \frac{n(n-1)}{2} \tag{1}$$

where n is the number of available electrodes. For the EIT oedometer in which 42 electrodes are present, this would result in a total of 861 independent measurements.

To obtain a suitable measuring sequence for the specific electrode configuration of the EIT oedometer, several synthetic tests have been performed by artificially generating conductivity maps to simulate different inclusions in soil samples. The synthetic voltage readings resulting from these conductivity maps were evaluated using the same forward operator used for the inverse solver. The reconstruction process was then performed on such data. No noise was added to the measurements at this stage in order to evaluate only the influence of the measuring sequence.

The selected sequence (Table 2) represents a combination of different protocols and it is conceived in order to measure potential differences in every portion of the cell avoiding redundancy. This sequence allows for a good reconstruction of the sample in most of the investigated situations. The total number of measures involved is 788, so that the acquisition of a single image can be performed in a few seconds using the acquisition device described in the previous section (depending on the selected frequency), an adequate time interval for most transient phenomena of interest.

TABLE 2—*Schematic representation of the adopted measuring sequence (electrodes numbers: 1 to 16 for circumferential ring, 17 to 29 for bottom cap and 30 to 42 for top cap).*

MEASURING SEQUENCE	
Current Injection	Voltage Measurements
Opposite electrodes on the boundary (1–9, 2–10, …)	Pair of electrodes on the two bases (17–18, 19–20, …, 30–31, …)
Opposite electrodes on the boundary (1–9, 2–10, …)	Pair of electrodes on the boundary (2–3, 2–4, …)
Opposite electrodes on the two bases (17–30, 18–31, …)	Opposite electrodes on the two bases (18–31, 19–32, …)
Opposite electrodes on bottom cap (17–29, 19–29, …)	Pair of electrodes on bottom cap (18–19, 18–20, …)
Opposite electrodes on top cap (30–42, 32–42, …)	Pair of electrodes on top cap (31–32, 31–33, …)

Preliminary Benchmark Tests

A series of simple experimental benchmark tests has been conducted in order to evaluate the potential of the cell in terms of 3D imaging through the tomographic reconstruction of the electrical conductivity field. Several homogeneous samples and samples with known conductive or resistive inclusions have been investigated to assess the accuracy in the 3D reconstruction. In particular, three benchmark tests, which reproduce different experimental disposition, are illustrated in the following:

- Test #1: Homogeneous sample
- Test #2: Resistive inclusion
- Test #3: Conductive inclusion

Tests #2 and #3 reproduce extreme conditions, since the adopted inversion method, which relies on the solution of an inverse problem with a regularized least-squares approach, is more suitable to detect smooth conductivity changes in space rather than the sharp variations associated with inclusions. Indeed, electric tomography has intrinsically a lower resolution than other more accurate imaging techniques and a smoothed inverted image will result, especially at the boundaries of the inclusion. Nevertheless, the smooth transitions associated with transient processes in geotechnical applications (such as infiltration or diffusion) represent far less severe situations for the tomographic imaging system.

In Test #1, the cell was filled with tap water to have a homogeneous sample. The objective of the test was to explore the ability of the method to reconstruct an uniform conductivity field and the accuracy in the determination of the average conductivity value. Figure 7 reports the reconstructed conductivity image, showing a quite homogeneous field with only minor defects. The average conductivity over the mesh was of 0.398 mS/cm, which compares very well with the value of 0.407 mS/cm, which was independently measured in the fluid with a conductimeter.

In Test #2, a resistive inclusion was placed in the cell, filled with the same tap water of Test #1. The inclusion was a Perspex® cylinder of 40 mm diameter and 25 mm height. The test was aimed at identifying both the position and dimensions of the target. In order to improve the interpretation, differential tomographic images are obtained subtracting the reconstructed conductivity field of Test #1 (Fig. 7) from the conductivity field obtained in Test #2. This strategy permits a clear identification of the inclusion and will be adopted also for the interpretation of the subsequent tests. In Fig. 8, cross sections at different sample heights of the differential conductivity map from Test #2 are reported together with a picture of the sample inside the cell. The scalebar reported in the figure refers to the three cross sections (the z axis is pointed from the bottom of the cell to the cap). Location and approximate dimensions of the resistive inclusion are correctly identified as an anomaly in the conductivity field. Nevertheless a small difference exists between the three cross sections of the imaged body as reconstructed, particularly for the one at $z=2$ cm. This is partially due to the fact that the inclusion is close to the lateral wall of the cell and a small "shadow" of the electric anomaly results in the reconstruction towards the boundary. Moreover the cross section at $z=2$ cm is in the proximity of the end of the inclusion (about two elements in the vertical direction), so that this section is particularly sensitive to the resolution of the electric tomography. This second effect is clearer in the overall 3D conductivity map of the sample (Fig. 9), which shows, however,

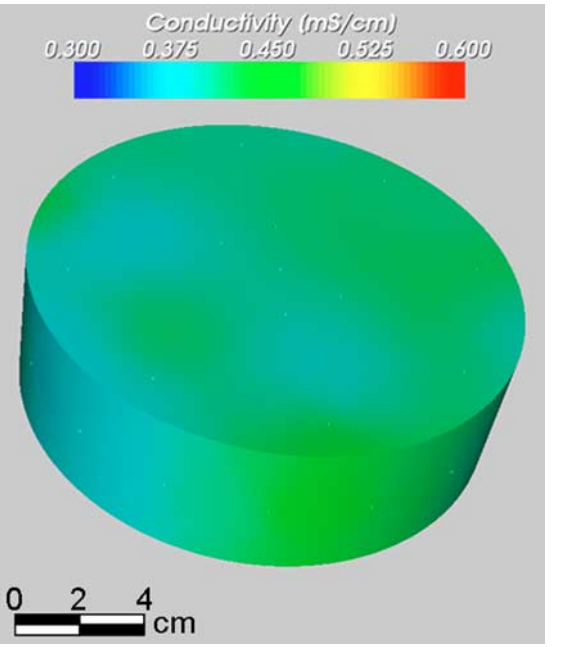

FIG. 7—*Test #1. Reconstructed conductivity for homogeneous sample (water).*

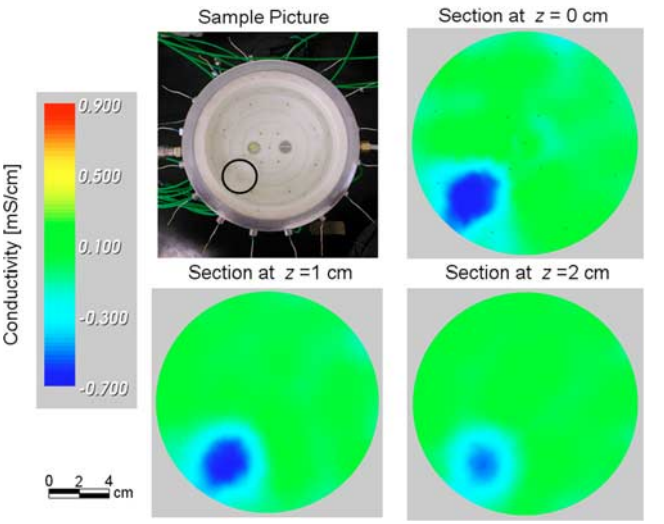

FIG. 8—*Test #2. Sample with resistive inclusion and cross section of the conductivity differences with respect to Test 1 (sample at different elevations).*

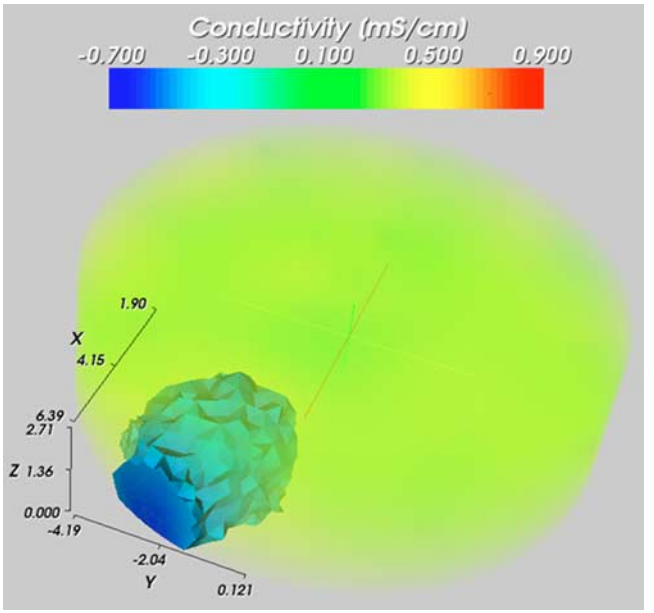

FIG. 9—*Test #2. Sample with resistive inclusion, 3D map of conductivity differences with respect to Test #1 with evidence of inclusion characteristics (quotes are in cm).*

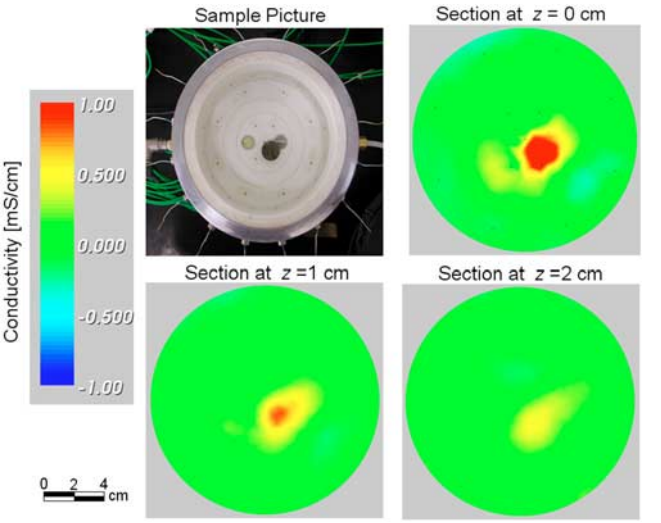

FIG. 10—*Test #3. Sample with conductive inclusion and cross section of the conductivity differences with respect to Test 1 (sample at different elevations).*

that the shape of the electrical anomaly (which is almost cylindrical with average dimensions 45.1 mm in diameter and 27.1 mm in height) matches very well the dimensions of the actual inclusion. It has also to be noted that a resistive inclusion represents a very challenging benchmark for the reconstruction process, indeed, in such a situation the electrical current has a preferential path in the more conductive background material; hence, the electric anomaly produced by the inclusion is very little and the successful inversion process represents a confirmation of the excellent performance of both acquisition device and reconstruction algorithm, whose effectiveness appears only slightly affected at the top of the resistive inclusion.

Test #3 reproduces a problem similar to Test #2, but with a conductive inclusion. The target in this case was a 20 mm diameter metallic sphere. As in the previous case, the inclusion is submerged in tap water and the differential tomographic reconstruction with respect to the results of Test #1 is reported in Fig. 10. Also in this case, the accuracy of the reconstruction process appears satisfactory within the resolution capabilities of ERT, proving the ability of the system to produce reliable results independently from the characteristics of the inclusion. Observing the contours (Fig. 10), it could be questioned that the inclusion is more similar to a cone, rather than a ball. This inconsistency can be attributed to the influence of the non-conductive bottom boundary that is in direct contact with the object and to the small dimensions of the inclusion.

It must be considered that these two tests reproduce very rare conditions in soil testing (i.e., the presence of a sharp anomalies in a specimen) that are extreme situations for the electric tomography and for which other imaging techniques could be more effective. However, in many applications to soil testing, smooth variations of the conductivity field inside the sample are expected and the implemented inversion method can be considered satisfactory.

Oedometer Test

Oedometer tests on real specimens have been performed to evaluate the overall performance of the testing equipment both for the mechanical aspects and for tomographic imaging. In the following the results of a test on a Ticino sand sample are presented. Ticino sand is an almost uniform quartz sand (mean particle size of 0.5 mm). The use of sand as testing material makes it possible a more consistent check of the equipment capabilities, because electrical conductivity is directly associated with soil porosity and interstitial fluid properties.

Indeed, quartz possesses an exceptionally large resistivity, so that it can be assumed, without reasonable errors, that electrical current is transported only by the movement of the free ions dissolved in the bulk solution (Mualen and Friedman 1991). Therefore, volumetric changes induced by the mechanical loads can be properly interpreted since it is particularly straightforward to interpret reconstructed conductivity patterns as porosity maps and to determine compaction characteristics.

Moreover in such material no important volume changes are expected; hence, it is not necessary to adapt the mesh used in the tomographic reconstruction to follow the evolution of sample height during the loading-unloading path. During the test, drainage was allowed only from the top cap in order to increase consolidation times.

Figure 11 gathers on the same plot the oedometer curve obtained through external LVDT measurements and the average con-

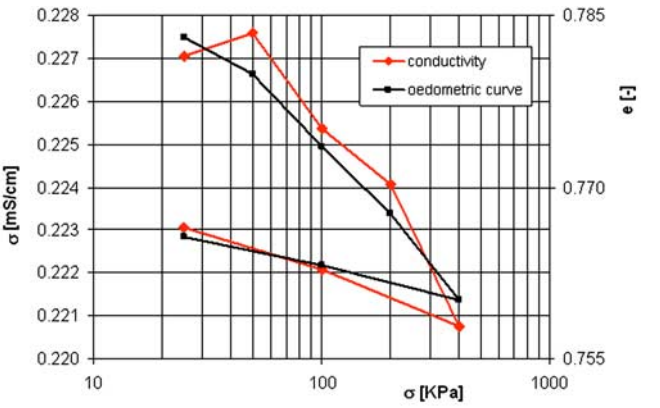

FIG. 11—*Oedometer test on Ticino sand.*

ductivity values inferred by ERT reconstructions performed at the end of each load increment. The oedometer curve has been evaluated accounting also for the frictional resistance offered by the o-ring of the top cap. The dependence of the electrical conductivity on load and load history reflects very well the mechanical behavior of the sample. As increasing stress leads the sample to a more compacted state, the overall conductivity is reduced because of reduction of the pore volume. Load removal inverts the trend but does not recover the previous conductivity values, because of the irreversible mechanical behavior. The only anomaly in the conductivity trend is observed in between 25 kpa and 50 kPa, where a small increase of the overall conductivity of the specimen is obtained. This can be associated with a possible redistribution of gaps and sand grain disposition by the applied load that determines preferential flow paths for electric conduction.

By introducing a suitable model relating the electrical conductivity of the fluid to the one of the porous medium, it is possible to interpret the results of the test in terms of porosity changes. Several relationships can be found in the literature relating electrical conductivity to porosity. Among them, the most widely used is the empirical rule due to Archie (1942). A generalized formula, adopted by several authors, for non-cemented fully resistive grains can be expressed as (e.g., Fricke 1924; Bruggeman 1935; Sen et al. 1981; Bussian 1983; Chin 2000):

$$\sigma_w = \frac{\sigma}{n^{\alpha}} \tag{2}$$

where σ is the conductivity of the porous medium, σ_w is the conductivity of the pore fluid, n is the porosity, and α is an exponent that depends on the characteristics of the system (Archie experimentally relates it to tortuosity of current flow paths and cementation; effective medium theories relate it to particle shape and ellipticity). According to the formulation proposed by Bruggeman (1935) on the basis of mixture theory, the constant α is equal to 3/2 for non-conductive spherical grains. The validity of this formula for Ticino sand has been verified in a previous study (Borsic et al. 2005).

The conductivity of the pore water, equal to 0.780 mS/cm, was measured by means of a conductimeter at the initial stage of the test. No major changes were expected during the evolution of the test because Ticino sand is constituted by clean quartz grains. Figure 12 shows the comparison of the experimental data and the values obtained with Bruggeman's formula for the different stages during the oedometer test, showing how it is possible to appreciate even very small changes in porosity.

During the test also the shear and compressional wave velocity of the specimen have been measured at different time steps using bender and pulser elements. As expected the velocity of P waves showed no significant variations in a saturated sample, whereas S wave velocity showed an increasing trend with external load (ranging from 120 m/s at 100 kPa to 180 m/s at 400 kPa).

The analysis of the reconstructed tomographic images can provide further elements with respect to the evolution of the tests. The conductivity maps of the sample at different time intervals for the same load increment, or for different load levels, are not of particular interest since images remain relatively uniform and the small overall conductivity reduction cannot be appreciated by visual inspection. Interesting differences arise instead in conductivity maps when the load is incremented or decremented. For example, Fig. 13 reports the image of a slice of the sample obtained as the difference between the reconstructed conductivity of the unloaded sample and

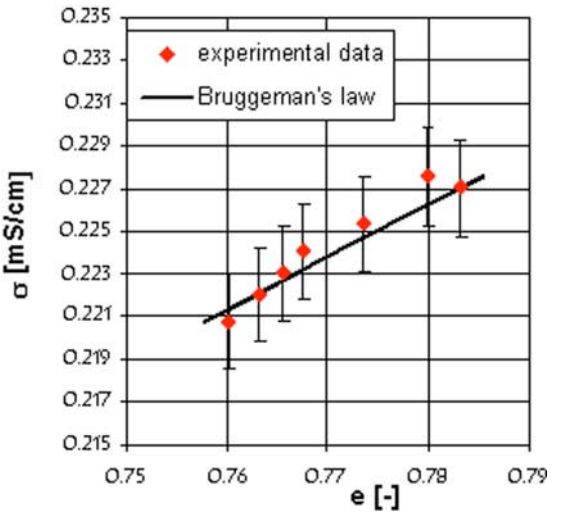

FIG. 12—*Conductivity void ratio interpretation of the oedometer test.*

the one of the tomography executed immediately after the application of the initial 25 kPa load. The application of the load leads to an increase of conductivity in the lower portion of the sample and to a reduction of conductivity in the upper portion, which clearly shows that consolidation is not uniform at this early stage and that it is influenced by ring friction effects and the upper drainage (only the top drainage line was opened). Hence, the upper drained part of the sample, subjected to a somewhat larger vertical effective stress, experiences a larger decrease of porosity and hence a decrease of conductivity. This feature clearly shows the potential of the reconstruction technique in monitoring the evolution of localized features during transient phenomena in soils.

Conclusions

There is a growing need for the development of new investigation techniques in laboratory experiments for non-conventional problems of hydro-chemo-mechanical nature in several engineering applications. In this respect the preliminary results obtained with this

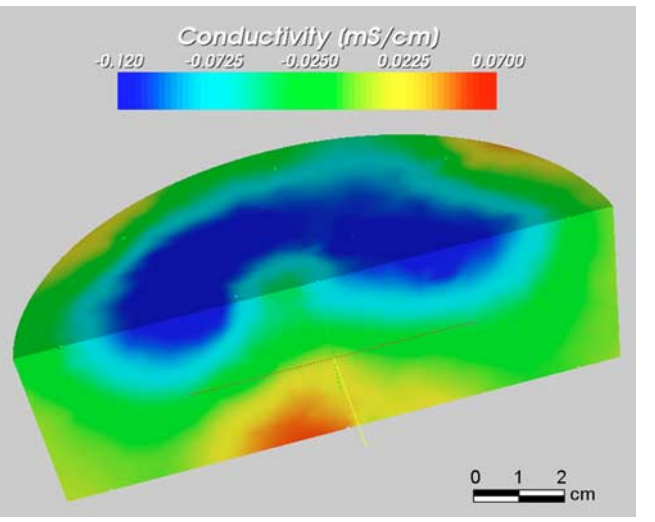

FIG. 13—*Oedometer test on Ticino sand. Conductivity differences between unloaded sample and first loading step.*

new measuring apparatus are promising for its application in geotechnical laboratories. The 3D electrical resistivity tomography implemented in the cell has proven effective in detecting both resistive and conductive target inclusions with good precision, as well as in monitoring porosity variations affecting the electrical conductivity of the medium.

The cell herein presented has the full potentiality to be used for a variety of applications related to transient phenomena in soil such as filtration/diffusion processes of different chemical species, monitoring the resulting conductivity field and preferential flow paths. The use of seismic wave velocity, as a complementary measurement technique, could, moreover, provide additional insight related to changes of the mechanical properties. Furthermore, the construction technology chosen for the allocation of the seismic sensors allows for an easy substitution of the sensors (e.g., for temperature monitoring). Alternatively, the same slots can be used to induce preferential flow paths of liquid infiltration or gas migration.

Finally, note that experiments in the laboratory can provide a meaningful link with *in situ* applications, where electrical resistivity tomography is currently used for site characterization and monitoring of several transient processes such as leakage from contaminated deposits and site remediation implementation.

Acknowledgments

Authors wish to thank Tomás Pérez for the fundamental contribution in the design and realization of the equipment and Claudia Festa for her valuable contribution in laboratory tests. The meetings for the equipment design have been financed by the integrated action Piemonte-Catalunya: Ajuts per a accions de cooperació i mobilitat de la Direcció General de Recerca de la Generalitat de Catalunya (ACI-2002-42 and ACI-2003-35) and by the Italian Ministry of International Affairs.

References

Amin, M. H. G., Chorley, R. J., Richards, K. S., Bache, B. W., Hall, L. D., and Carpenter, T. A., 1993, "Spatial and Temporal Mapping of Water in Soil by Magnetic Resonance Imaging," *Hydrolog. Process.*, Vol. 7, pp. 279–286.

Anderson, S. H., Peyton, R. L., Wigger, J. W., and Gantzer, C. J., 1992, "Influence of Aggregate Size on Solute Transport as Measured Using Computed Tomography," *Geoderma*, Vol. 53, pp. 387–398.

Archie, G. E., 1942, "The Electrical Resistivity Log as an Aid to Determining Some Reservoir Characteristics," *Trans. AIME*, Vol. 146, pp. 54–63.

Berryman, J. G., 1995, *A Handbook of Physical Constants*, American Geophysical Union, Washington DC, Chap. 6, pp. 205–228.

Binley, A., Shaw, B., and Henry-Poulter, S., 1996, "Flow Pathways in Porous Media: Electrical Resistance Tomography and Dye Staining Image Verification," *Meas. Sci. Technol.*, Vol. 7, pp. 384–390.

Blewett, J., McCarter, W. J., Chrisp, T. M., and Starrs, G., 2001, "Monitoring Sedimentation of a Clay Slurry," *Geotechnique*, Vol. 51, No. 8, pp. 723–728.

Borsic, A., 2002, "Regularlization Methods for Imaging from Electrical Measurements," Ph.D. Thesis, School of Engineering Oxford Brookes University, Oxford.

Borsic, A., Comina, C., Lancellotta, R., Foti, S., and Musso, G., 2005, "Imaging Heterogeneities in Sand Samples with ERT: Laboratory Results," *Geotechnique*, Vol. 50, No. 7, pp. 539–547.

Brignoli, E. G. M., Gotti, M., and Stokoe, K. H., 1996, "Measurements of Shear Waves in Laboratory Specimens by Means of Piezoelectric Transducers," *Geotech. Test. J.*, Vol. 19, pp. 384–397.

Bruggeman, D. A. G., 1935, "Berechnung Verschiedener Physikalischer Konstanten Von Heterogenen Substanten," *Ann. Phys.*, Vol. 24, pp. 636–679.

Bussian, A. E., 1983, "Electrical Conductance in a Porous Medium," *Geophysics*, Vol. 48, pp. 1258–1268.

Chin, P. D., 2000, "Electrical Properties of Sedimentary Rocks Having Interconnected Water-Saturated Pore Spaces," *Geophysics*, Vol. 65, No. 4, pp. 1093–1097.

Comina, C., 2005, "Imaging Heterogeneities and Diffusion in Sand Samples-Electric and Seismic Methods," Ph.D. Thesis, Politecnico di Torino, Torino.

Comina, C., Foti, S., Lancellotta, R., Musso, G., and Borsic, A., 2005, "Imaging Heterogeneities and Diffusion in Sand Samples," Proceedings of the 11th International Conference of the International Association of Computer Methods and Advances in Geomechanics IACMAG2005, Torino, Vol. 2, pp. 27–34.

Damasceno, V. M., and Fratta, D., 2006, "Chemical Diffusion Detection in a Porous Media Using Electrical Resistance Tomography," ASCE Geotechnical Special Publication (GSP) 149: *Site and Geomaterial Characterization* 2006 GeoShanghai International Conference, Shanghai, China, ASCE, Roston, VA, pp. 174–181.

Fricke, H., 1924, "A Mathematical Treatment of the Electrical Conductivity and Capacity of Disperse Sistems: The Electric Conductivity of a Suspension of Homogeneous Spheroids," Department of Bio-physics, Cleveland Clinic Foundation, pp. 575–587.

Gens, A., and Alonso, E. E., 1992, "A Framework for the Behaviour of Unsaturated Expansive Clays," *Can. Geotech. J.*, Vol. 29, pp. 1013–1032.

Hedburg, S. A., Knight, R. J., MacKay, A. L., and Whittall, K. P., 1993, "The Use of Nuclear Magnetic Resonance for Studying and Detecting Hydrocarbon Contaminants in Porous Rocks," *Water Resour. Res.*, Vol. 29, pp. 1163–70.

Jinguuji, M., Toprak, S., and Kunimatsu, S., 2007, "Visualization Technique for Liquefaction Process in Chamber Experiments by Using Electrical Resistivity Monitoring," *Soil Dyn. Earthquake Eng.*, Vol. 27, pp. 191–199.

Jovicic, V., Coop, M. R., and Simic, M., 1996, "Objective Criteria for Determining Gmax from Bender Elements Tests," *Geotechnique*, Vol. 46, pp. 357–362.

Kamon, M., Endo, K. E., Katsumi, T., 2003, "Measuring the K-S-P Relations on Dnapls Migration," *Eng. Geol. (Amsterdam)*, Vol. 70, pp. 351–363.

Lee, J.-S., and Santamarina, J. C., 2005, "Bender Elements-Performance and Signal Interpretation," *J. Geotech. Geoenviron. Eng.*, Vol. 131, pp. 1063–1070.

McCarter, W. J., and Desmazes, P., 1997, "Soil Characterization Using Electrical Measurements," *Geotechnique*, Vol. 47, No. 1, pp. 179–183.

Mitchell, J. K., 1993, *Fundamentals of Soil Behavior*, 2nd Ed., John Wiley and Sons, New York.

Mualen, Y., and Friedman, P., 1991, "Theoretical Prediction of

Electrical Conductivity in Saturated and Unsaturated Soil," *Water Resour. Res.*, Vol. 27, pp. 2771–2777.

Murphy, S. C., Stanley, S. J., Rhodes, D., and York, T. A., 2006, "3D Electrical Tomographic Imaging Using Vertical Arrays of Electrodes," *Meas. Sci. Technol.*, Vol. 17, pp. 3053–3065.

Noel, M., and Xu, B., 1991, "Archaeological Investigation by Electrical Resistance Tomography: A Preliminary Study," *Geophys. J. Int.*, Vol. 107, pp. 95–102.

Olsen, P. A., Binley, A., Henry-Poulter, S., and Tych, W., 1999, "Characterizing Solute Transport in Undisturbed Soil Cores Using Electrical and X-Ray Tomographic Methods," *Hydrol. Process.*, Vol. 13, pp. 211–221.

Peyton, R. L., Haeffner, B. A., Anderson, S. H., and Gantzer, C. J., 1992, "Applying X-Ray CT to Measure Macropore Diameters in Undisturbed Soil Cores," *Geoderma*, Vol. 53, pp. 329–40.

Pfannkuch, H. O., 1969, "On the Correlation of Electrical Conductivity Properties of Porous Systems with Viscous Flow Transport Coefficients," Proc. IAHR 1st Int. Symp. Fundamentals of Transport Phenomena in Porous Media, Haifa.

Reynolds, J. M., 1997, *An Introduction to Applied and Environmental Geophysics*, John Wiley and Sons, New York.

Rodríguez-Rey, A., Ruiz de Argandoña, V. G., Calleja, L., Suárez del Río, L. M., and Velorio, C., 2006, "Consolidants Influence on Sandstone Capillarity. X-Ray Study," *Advances in X-ray Tomography for Geomaterials*. J. Desrues, G. Viggiani, and P. Bésuelle, Eds., ISTE Ltd, London, UK, pp. 381–387.

Rolland, S., Stemmelen, D., Moyne, C., and Masrouri, F., 2005, "Experimental Hydraulic Measurements in an Unsaturated Swelling Soil Using the Dual-Energy Gamma-Ray Technique,#x201D; Proc. Int. Symposium on Advanced Experimental Unsaturated Soil Mechanics, Trento, Italy, 27–29 June 2005, *Advanced Experimental Unsaturated Soil Mechanics*, A. Tarantino, E. Romero, and Y. J. Cui, Eds., Taylor & Francis Group, London, pp. 305–310.

Romero, E., Lloret, A., and Gens, A., 1995, "Development of a New Suction and Temperature Controlled Oedometer," Proc. 1st Int. Conf. on Unsaturated Soils, Paris. E. E. Alonso, and P. Delage, Eds., Balkema / Presses des Ponts et Chaussées, Vol. 2, pp. 553–559.

Sambuelli, L., Lollino, G., Morelli, G., Socco, L. V., and Bidone, L., 2002, "First Experiments on Solid Transport Estimation in River-Flow by Fast Impedance Tomography," 8th EEGS-ES meeting, Aveiro, Portugal, CD-rom.

Sambuelli, L., Socco, L. V., Godio, A., Nicolotti, G., and Martins, R., 2003, "Ultrasonic, Electric and Radar Measurements for Living Trees Assessment," *Boll. Geofis. Teor. Appl.*, Vol. 44, pp. 253–279.

Santamarina, J. C., and Fam, M., 1995, "Changes in Dielectric Permittivity and Shear Wave Velocity During Concentration Diffusion," *Can. Geotech. J.* Vol. 32, No. 4, pp. 647–659.

Sen, P. N., Scala, C., and Cohen, M. H., 1981, "A Self-Similar Model for Sedimentary Rocks with Application to the Dielectric Constant of Fused Glass Beads," *Geophysics*, Vol. 46, pp. 781—795.

Somersalo, E., Cheney, M., and Isaacson, D., 1992, "Existence and Uniqueness for Electrode Models for Electric Current Computed Tomography," *SIAM J. Appl. Math.*, Vol. 52, pp. 1023–1040.

Van Geet, M., Volckaert, G., and Roels, S., 2005, "The Use of Microfocus X-Ray Computed Tomography in Characterising the Hydration of a Clay Pellet/Powder Mixture," *Appl. Clay Sci.*, Vol. 29, pp. 73–87.